



## NRC Publications Archive Archives des publications du CNRC

### **A Continuous second order sensitivity equation method for time-dependent incompressible laminar flows**

Ilinca, F.; Pelletier, D.; Borggaard, J.

This publication could be one of several versions: author's original, accepted manuscript or the publisher's version. /  
La version de cette publication peut être l'une des suivantes : la version prépublication de l'auteur, la version acceptée du manuscrit ou la version de l'éditeur.

#### **Publisher's version / Version de l'éditeur:**

*[Papers presented at the joint 35th AIAA Fluid Dynamics Conference & Exhibit, 36th AIAA Plasmadynamics and Lasers Conference, 4th AIAA Theoretical Fluid Mechanics Meeting, 38th AIAA Thermophysics Conference, 23rd AIAA Applied*

#### **NRC Publications Record / Notice d'Archives des publications de CNRC:**

<https://nrc-publications.canada.ca/eng/view/object/?id=a1143510-f311-4d79-bc4f-dceb1b8cb7c9>

<https://publications-cnrc.canada.ca/fra/voir/objet/?id=a1143510-f311-4d79-bc4f-dceb1b8cb7c9>

Access and use of this website and the material on it are subject to the Terms and Conditions set forth at

<https://nrc-publications.canada.ca/eng/copyright>

READ THESE TERMS AND CONDITIONS CAREFULLY BEFORE USING THIS WEBSITE.

L'accès à ce site Web et l'utilisation de son contenu sont assujettis aux conditions présentées dans le site

<https://publications-cnrc.canada.ca/fra/droits>

LISEZ CES CONDITIONS ATTENTIVEMENT AVANT D'UTILISER CE SITE WEB.

**Questions?** Contact the NRC Publications Archive team at

PublicationsArchive-ArchivesPublications@nrc-cnrc.gc.ca. If you wish to email the authors directly, please see the first page of the publication for their contact information.

**Vous avez des questions?** Nous pouvons vous aider. Pour communiquer directement avec un auteur, consultez la première page de la revue dans laquelle son article a été publié afin de trouver ses coordonnées. Si vous n'arrivez pas à les repérer, communiquez avec nous à PublicationsArchive-ArchivesPublications@nrc-cnrc.gc.ca.



17th AIAA Computational Fluid Dynamics Conference  
6-9 Jun 2005 Toronto / ON

# A Continuous Second Order Sensitivity Equation Method for Time-Dependent Incompressible Laminar Flows

F. Ilinca\*

*National Research Council, Boucherville (Québec), Canada, J4B 6Y4*

D. Pelletier†

*École Polytechnique de Montréal, Montréal (Québec), Canada, H3C 3A7*

and

J. Borggaard‡

*Virginia Tech, Blacksburg, Virginia 24061-0531*

This paper presents a general formulation of the continuous sensitivity equation method (SEM) for computing first and second order sensitivities of time-dependent, incompressible laminar flows. The formulation accounts for complex parameter dependence and is suitable for a wide range of problems. The SEM formulation is verified on a problem with a closed form solution. Systematic grid convergence studies confirm the theoretical rates of convergence in both space and time. The methodology is then applied to pulsed flow around a square cylinder. The flow starts with symmetrical vortex shedding then transitions to the traditional Von Karman street (alternate vortex shedding). Sensitivities are used to demonstrate fast evaluation of nearby flows. The accuracy of nearby flows is much improved when second order sensitivities are used. For the uniform flow around a circular cylinder the sensitivity of the Strouhal number with respect to the Reynolds number agrees well with the computed and experimental  $St-Re$  relationship.

## Nomenclature

$f$	frequency of vortex shedding
$\mathbf{f}$	body force
$\mathbf{F}^N$	imposed surface force
$\mathbb{I}$	identity tensor
$\hat{\mathbf{n}}, \hat{\mathbf{t}}$	normal and tangent unit vectors
$p$	pressure
$Re$	Reynolds number
$St$	Strouhal number
$s_x$	sensitivity of the dependent variable $x$
$t$	time
$\mathbf{t}$	surface traction
$\mathbf{u}$	velocity
$u, v$	$x$ and $y$ velocity components
$U_D$	imposed boundary velocity
$x, y$	Cartesian coordinates

\*Research Officer, Industrial Materials Institute

†Canada Research Chair, Mechanical engineering, Associate Fellow AIAA

‡Associate Professor, Interdisciplinary Center for Applied Mathematics, Senior Member AIAA

$\Gamma$	boundary
$\mu$	viscosity
$\rho$	density
$\tau$	stress tensor
$\Omega$	computational domain

## I. Introduction

An engineer using CFD for design must answer two questions: are the flow predictions obtained with CFD accurate enough for design purposes? and what are the consequences of changing the parameters controlling the system (boundary conditions, shape parameters, etc.)? This paper presents a general continuous sensitivity equation method for time-dependent incompressible laminar flows as a means of answering the latter question. The former issue is best dealt with by a comprehensive validation study including systematic time-step and grid refinement studies and comparison to experimental measurements.

A sensitivity is the derivative of a dependent variable with respect to a design parameter. For the flow around an airfoil,  $\frac{\partial u}{\partial \alpha}$  is the sensitivity of the velocity with respect to the airfoil angle of attack. It expresses how the velocity field responds to perturbations of  $\alpha$  around its nominal value. Sensitivity information can also provide fast evaluation of nearby flows without resorting to a full blown flow re-analysis. This is done via Taylor series in parameter space, and is especially useful to answer *what if questions* for complex flows. Finally, sensitivity information can serve to cascade input data uncertainty through a CFD code to yield uncertainty estimates of the flow response. In both cases cost-effectiveness is achieved because sensitivities are obtained at a fraction of the cost of computing the flow.

There are several means of computing flow sensitivities: finite differences of flow solutions, the complex step method,<sup>1</sup> automatic differentiation,<sup>2</sup> and sensitivity equation methods.<sup>3-5</sup> The first option is costly because the problem must be solved for two or more values of each parameter of interest. Furthermore, technical problems arise because non matching meshes are obtained for different values of a shape parameter. The complex-step method is code invasive: it requires a complete rewrite of the software in complex variables. While this can be automated, it has a significant impact on performance. Automatic differentiation is equivalent to differentiating the discrete equations to generate a system of equations for the discrete sensitivities. It is powerful because it automatically generates the code for calculating sensitivities. In many cases, implementation requires human intervention to ensure efficiency of the code. Approaches to calculating sensitivities also differ depending on the order of the operations of approximation and differentiation. In the *discrete* sensitivity equation approach, the total derivative of the flow approximation with respect to the parameter is calculated,<sup>6</sup> whereas in the *continuous* sensitivity equation method (SEM) one differentiates the continuum equations to yield differential equations for the continuous sensitivities.<sup>3</sup> See Hien et al.<sup>7</sup> for a discussion of the two approaches. We have adopted the latter approach.

Sensitivity analysis is a more advanced field in solid mechanics than in fluid dynamics. Indeed, textbooks have been written on sensitivity analysis of structures.<sup>6,7</sup> To our knowledge there is only one book on sensitivity analysis of flow problems.<sup>4</sup> It is recent and more specialized than structural mechanics books. Gunzburger<sup>8</sup> discusses sensitivity analysis in the context of flow control and optimization.

Automatic differentiation for first-order flow sensitivities is discussed by Sherman<sup>9</sup> and Putko.<sup>2</sup> Continuous SEMs may be found in Godfrey,<sup>10,11</sup> Borggaard,<sup>3</sup> Limache<sup>12</sup> and Turgeon<sup>13</sup> for aerodynamics applications. Application to heat conduction is reported by Blackwell.<sup>14</sup> Sensitivities for incompressible flows with heat transfer may be found in several references.<sup>5,15-17</sup> Sensitivity analysis for turbulence models is detailed in the works by Godfrey<sup>11</sup> and Turgeon.<sup>18,19</sup> Solution of the sensitivity equations for the transient incompressible flow of non-Newtonian fluids is presented by Ilinca.<sup>20</sup> A wide variety of flow regimes were treated by the authors.<sup>5,16,17,19,21,22</sup> This body of work has shown that sensitivities provide an enriched base of information on which to develop an understanding of complex flow problems. The work presented here is an extension to first and second order sensitivities for time-dependent flows, of the methodology developed previously for steady state flows.<sup>5,17</sup>

The paper is organized as follows. First, we present the equations describing time-dependent laminar flow along with their boundary and initial conditions. The first and second order sensitivity equations and their boundary/initial conditions are then described in detail. The methodology and its finite element solver are verified on a problem possessing a closed form solution. The approach is then applied to pulsed flow

around a square cylinder. Several uses of sensitivities are demonstrated. For the uniform flow past a circular cylinder emphasis is put on the  $St-Re$  relationship and the computed sensitivity of the Strouhal number. The paper ends with conclusions.

## II. Flow equations

### A. Navier-Stokes Equations

The flow regime of interest is modeled by the momentum and continuity equations:

$$\rho \frac{\partial \mathbf{u}}{\partial t} + \rho \mathbf{u} \cdot \nabla \mathbf{u} = -\nabla p + \mathbf{f} + \nabla \cdot \left[ \mu \left( \nabla \mathbf{u} + (\nabla \mathbf{u})^T \right) \right] \quad (1)$$

$$\nabla \cdot \mathbf{u} = 0 \quad (2)$$

where  $\rho$  is the density,  $\mathbf{u}$  is the velocity,  $p$  is the pressure,  $\mu$  is the viscosity,  $t$  represents time and  $\mathbf{f}$  is a body force. The above system is closed with a proper set of initial conditions

$$\mathbf{u}(\mathbf{x}, t = 0) = U_0(\mathbf{x}) \text{ in } \Omega \quad (3)$$

and Dirichlet and Neumann boundary conditions

$$\mathbf{u}(\mathbf{x}, t) = U_D(\mathbf{x}, t) \text{ on } \Gamma_D. \quad (4)$$

$$\mathbf{t} = [-p\mathbb{I} + 2\mu\boldsymbol{\gamma}(\mathbf{u})] \cdot \hat{\mathbf{n}} = \mathbf{F}^N \text{ on } \Gamma_N \quad (5)$$

where  $U_D$  is the value of the velocity imposed on the boundary  $\Gamma_D$ ,  $\mathbb{I}$  is the identity tensor,  $\boldsymbol{\gamma}(\mathbf{u}) = (\nabla \mathbf{u} + \nabla \mathbf{u}^T)/2$  is the shear rate tensor and  $\mathbf{F}^N$  is the imposed boundary value of the surface traction force  $\mathbf{t}$ .

## III. Sensitivity Equations

### A. General Formulation of First Order Sensitivity Equations

The continuous sensitivity equations (CSE) are derived formally by implicit differentiation of the flow equations (1) and (2) with respect to parameter  $a$ . We treat the variable  $\mathbf{u}$  as a function of space, time and of the parameter  $a$ . This dependence is denoted as  $\mathbf{u}(\mathbf{x}, t; a)$ . Defining the flow sensitivities as the partial derivatives  $s_u^a = \frac{\partial \mathbf{u}}{\partial a}$  and  $s_p^a = \frac{\partial p}{\partial a}$ , and denoting the derivatives of the fluid properties and other flow parameters by a (') and the subscript  $a$ , differentiation of equations (1) and (2) yields

$$\rho'_a \left( \frac{\partial \mathbf{u}}{\partial t} + \mathbf{u} \cdot \nabla \mathbf{u} \right) + \rho \left( \frac{\partial s_u^a}{\partial t} + \mathbf{u} \cdot \nabla s_u^a + s_u^a \cdot \nabla \mathbf{u} \right) = -\nabla s_p^a + \mathbf{f}'_a \quad (6)$$

$$+ \nabla \cdot \left[ \mu'_a \left( \nabla \mathbf{u} + (\nabla \mathbf{u})^T \right) + \mu \left( \nabla s_u^a + (\nabla s_u^a)^T \right) \right] \quad (7)$$

$$\nabla \cdot s_u^a = 0.$$

### B. General Formulation of Second Order Sensitivity Equations

The same method is applied to obtain second order sensitivity equations. We consider here two independent parameters  $a$  and  $b$ . Thus,  $\mathbf{u}$  can be written as  $\mathbf{u}(\mathbf{x}, t; a, b)$ . Second order flow sensitivities are defined as the partial derivatives  $s_u^{ab} = \frac{\partial^2 \mathbf{u}}{\partial a \partial b}$  and  $s_p^{ab} = \frac{\partial^2 p}{\partial a \partial b}$ , and denoting the derivatives of the fluid properties and other

flow parameters by a (") and the subscript  $ab$ , differentiation of equations (1) and (2) yields

$$\begin{aligned} \rho''_{ab} \left( \frac{\partial \mathbf{u}}{\partial t} + \mathbf{u} \cdot \nabla \mathbf{u} \right) + \rho'_a \left( \frac{\partial s_{\mathbf{u}}^b}{\partial t} + \mathbf{u} \cdot \nabla s_{\mathbf{u}}^b + s_{\mathbf{u}}^b \cdot \nabla \mathbf{u} \right) + \\ \rho'_b \left( \frac{\partial s_{\mathbf{u}}^a}{\partial t} + \mathbf{u} \cdot \nabla s_{\mathbf{u}}^a + s_{\mathbf{u}}^a \cdot \nabla \mathbf{u} \right) + \\ \rho \left( \frac{\partial s_{\mathbf{u}}^{ab}}{\partial t} + \mathbf{u} \cdot \nabla s_{\mathbf{u}}^{ab} + s_{\mathbf{u}}^b \cdot \nabla s_{\mathbf{u}}^a + s_{\mathbf{u}}^a \cdot \nabla s_{\mathbf{u}}^b + s_{\mathbf{u}}^{ab} \cdot \nabla \mathbf{u} \right) = -\nabla s_p^{ab} + f''_{ab} + \end{aligned} \quad (8)$$

$$\begin{aligned} \nabla \cdot \left[ \mu''_{ab} \left( \nabla \mathbf{u} + (\nabla \mathbf{u})^T \right) + \mu'_b \left( \nabla s_{\mathbf{u}}^a + (\nabla s_{\mathbf{u}}^a)^T \right) + \right. \\ \left. \mu'_a \left( \nabla s_{\mathbf{u}}^b + (\nabla s_{\mathbf{u}}^b)^T \right) + \mu \left( \nabla s_{\mathbf{u}}^{ab} + (\nabla s_{\mathbf{u}}^{ab})^T \right) \right] \\ \nabla \cdot s_{\mathbf{u}}^{ab} = 0. \end{aligned} \quad (9)$$

### C. Initial and Boundary Conditions

Initial conditions for the sensitivity equations are obtained by implicit differentiation of equation (3)

$$s_{\mathbf{u}}^a(\mathbf{x}, t = 0) = \frac{\partial U_0}{\partial a}(\mathbf{x}) \quad \text{in } \Omega, \quad (10)$$

$$s_{\mathbf{u}}^{ab}(\mathbf{x}, t = 0) = \frac{\partial^2 U_0}{\partial a \partial b}(\mathbf{x}) \quad \text{in } \Omega. \quad (11)$$

Dirichlet condition are obtained in a similar manner and can be written as:

$$s_{\mathbf{u}}^a = \frac{\partial U_D}{\partial a} \quad \text{on } \Gamma_D, \quad (12)$$

$$\frac{\partial t}{\partial a} = [-s_p^a \mathbb{I} + 2(\mu \gamma(s_{\mathbf{u}}^a) + \mu'_a \gamma(\mathbf{u}))] \cdot \hat{\mathbf{n}} = \frac{\partial F^N}{\partial a} \quad \text{on } \Gamma_N \quad (13)$$

for the first order sensitivities, and:

$$s_{\mathbf{u}}^{ab} = \frac{\partial^2 U_D}{\partial a \partial b} \quad \text{on } \Gamma_D, \quad (14)$$

$$\frac{\partial^2 t}{\partial a \partial b} = [-s_p^{ab} \mathbb{I} + 2(\mu \gamma(s_{\mathbf{u}}^{ab}) + \mu'_a \gamma(s_{\mathbf{u}}^b) + \mu'_b \gamma(s_{\mathbf{u}}^a) + \mu''_{ab} \gamma(\mathbf{u}))] \cdot \hat{\mathbf{n}} = \frac{\partial^2 F^N}{\partial a \partial b} \quad \text{on } \Gamma_N \quad (15)$$

for the second order sensitivities.

## IV. Implementation

The flow equations and the CSE are solved on three-dimensional meshes by a Streamline-Upwind Petrov Galerkin (SUPG) finite element method.<sup>23</sup> Time is discretized by an implicit Euler scheme. The equations are linearized with Newton's method and discretized with the 4-node element using linear interpolants for the velocity and pressure. The same element is used to solve the sensitivity equations. Element matrices are constructed using a numerical Jacobian technique and assembled in a compressed sparse row format. Flow and sensitivity global systems are solved by BiCG stabilized iterative methods.

## V. Numerical Results

In this section the numerical approach is first verified using the method of manufactured solutions (MMS)<sup>24</sup> and then applied to the case of time-dependent pulsed flow around square and circular cylinders and to the uniform flow around a circular cylinder. In the verification case, direct differentiation of the manufactured solution provides closed-form expressions for the sensitivities. A grid convergence study is performed to assess the accuracy of the flow and sensitivity solutions.

## A. Verification

We use the following expressions for the velocity components taken from the Stommel ocean flow model<sup>25</sup>

$$u(x, y) = \frac{\mathcal{F}}{R} \cos\left(\frac{\pi y}{b}\right) \left[ C_1 e^{k_1 x} + C_2 e^{k_2 x} - 1 \right] \quad (16)$$

$$v(x, y) = -\frac{b \mathcal{F}}{\pi R} \sin\left(\frac{\pi y}{b}\right) \left[ C_1 k_1 e^{k_1 x} + C_2 k_2 e^{k_2 x} \right] \quad (17)$$

with

$$k_{1,2} = -\frac{D\beta}{2R} \pm \sqrt{\left(\frac{D\beta}{2R}\right)^2 + \left(\frac{\pi}{b}\right)^2}, \quad (18)$$

and

$$C_1 = \frac{1 - e^{k_2 \lambda}}{e^{k_1 \lambda} - e^{k_2 \lambda}}, \quad C_2 = \frac{e^{k_1 \lambda} - 1}{e^{k_1 \lambda} - e^{k_2 \lambda}}. \quad (19)$$

The same problem was used by Hristova et al.<sup>26</sup> to verify the 2D solution of the flow and first order sensitivity equations. Figures 1(a) and 1(b) are sketches of the flow field for  $\beta = 0$  and  $\beta \neq 0$ . Also shown is the shape of the wind force  $\mathcal{F}$ . The original Stommel solution is for a steady-state flow. By taking

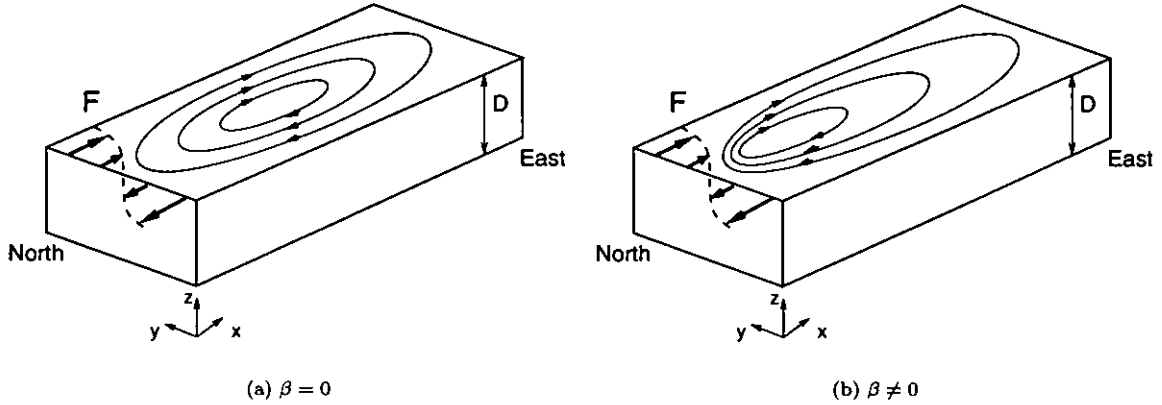


Figure 1. Flow pattern for ocean-like flow

$$\mathcal{F} = F \sin(\pi t) \quad (20)$$

we generate a time-dependent velocity field suitable for verification. Finally, we choose the pressure to be:

$$p(x, y) = 2\mu \frac{\partial v}{\partial y} = -2 \frac{\mathcal{F}}{R} \cos\left(\frac{\pi y}{b}\right) \left[ C_1 k_1 e^{k_1 x} + C_2 k_2 e^{k_2 x} \right]. \quad (21)$$

so that a zero normal traction ( $F_y^N = 0$  in Eq. 15) may be imposed on the top and bottom boundaries of the computational domain as shown on Figure 2. These expressions are substituted in the Navier-Stokes equations to define the body force  $\mathbf{f}$  ensuring that the momentum equations (1) are satisfied.<sup>26</sup>

The meaning and values of the various parameters are given in Table 1. For simplicity, the length scale is taken as  $L^* = b = 2\pi \times 10^6 m$  while the time-scale is  $T^* = 1/\beta L^*$ .

The computational domain and boundary conditions are shown on Figure 2. A grid and time step convergence study is carried out for the flow and its first and second order sensitivities with respect to the following two parameters: the Coriolis coefficient  $\beta$  and the friction coefficient  $R$ . Analytical expressions for the sensitivities are obtained by direct differentiation of equations (16) to (21). The required source terms  $\mathbf{f}'$  and  $\mathbf{f}''$  in the sensitivity equations are obtained by first and second order differentiation of  $\mathbf{f}$  in Eq. (1). The grid refinement study reported here is performed for  $\beta = 0$ . Similar results were obtained with  $\beta \neq 0$ . The mesh and time steps for the grid sequence are reported in Table 2. With this data one expects the true error at the final time of the simulation to be reduced by a factor of 2 from one mesh to the next. Figures

**Table 1.** Parameters of the “ocean-like” manufactured solution.

Parameter	dimensional	non-dimensional
latitude, $b$	$2\pi \times 10^6 m$	1.00
longitude, $\lambda$	$10^7 m$	1.59
depth, $D$	$200m$	$3.1831 \times 10^{-5}$
wind force, $F$	$0.3 \times 10^{-5} m^2 s^{-2}$	$1.9249 \times 10^{-11}$
friction coefficient, $R$	$0.6 \times 10^{-3} m s^{-1}$	$1.5198 \times 10^{-6}$
Coriolis effect, $\beta$	$10^{-11} m^{-1} s^{-1}$	1.00

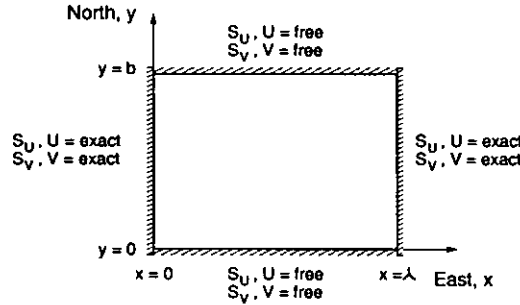


**Figure 2.** Verification problem: Computational domain.

3(a) and 3(b) show the results for the velocity, pressure and their sensitivities with respect to  $\beta$  and  $R$ . The results show clearly that the flow and sensitivity solvers exhibit their theoretical rates of convergence. Hence, the code is verified in the sense of Roache.<sup>24</sup> In the present case,  $\beta = 0$ , and the solution for the sensitivities with respect to  $R$  are obtained by multiplying the flow solution by  $-1/R$  for the first order sensitivities and by  $1/R^2$  for the second order sensitivities. We would therefore expect the errors for the first and second order sensitivities with respect to  $R$  to behave as the error of the flow solution. Results in figures 3(a) and 3(b) show that the errors of the sensitivities with respect to  $R$  are almost superimposed over the values for the solution error.

**Table 2.** Mesh size and time steps for verification problem.

Mesh	$h$	$\Delta t$
1	0.2	0.1
2	0.1	0.05
3	0.05	0.025
4	0.025	0.0125
5	0.0125	0.00625

## B. Pulsed flow around a square cylinder

### 1. Problem statement

The computational domain and boundary conditions for this problem are shown on Figure 4(a). Because the problem is two-dimensional only a slab was meshed with 3D tetrahedral elements. The mesh is shown on Figure 4(b) and was designed to provide adequate flow and sensitivity resolution. The inflow velocity

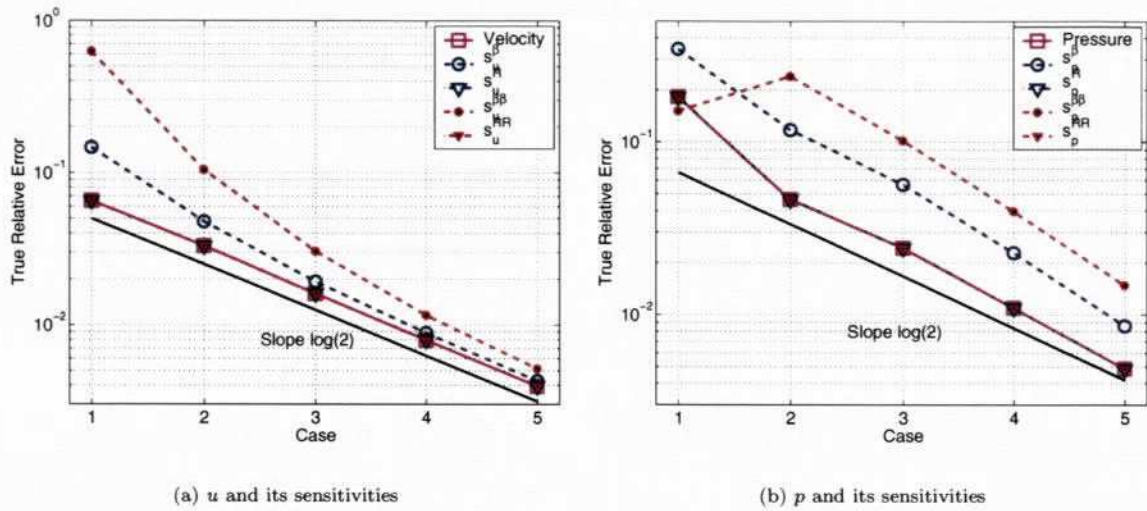


Figure 3. Verification problem: Convergence of  $u$ ,  $p$  and their sensitivities.

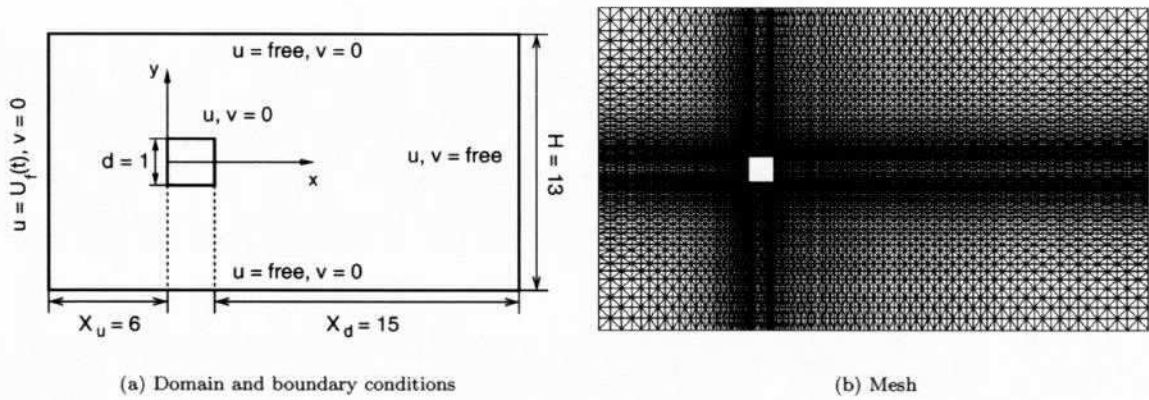


Figure 4. Pulsed flow around a square cylinder: Definition and mesh.

varies in time according to:

$$U_f(t) = U_0 \left( 1 + \alpha \sin \frac{2\pi t}{T_\alpha} \right) \quad (22)$$

where  $U_0$  is the time mean value of the free-stream velocity,  $\alpha$  the amplitude of the sinusoidal variation, and  $T_\alpha$  its period. These parameters are set to

$$U_0 = 1, \quad \alpha = 0.4, \quad T_\alpha = 4. \quad (23)$$

The initial conditions are obtained from a steady state solution of the flow and sensitivity equations. The Reynolds number  $Re = \rho U_0 d/\mu$  is set to 100.

The time-step is set to  $\Delta T = 0.025$  following the work of Sohankar.<sup>27</sup> This leads to 160 time-steps per period of the inflow boundary condition ( $T_\alpha = 4$ ). Sensitivities are computed with respect to  $U_0$ ,  $\alpha$ , and  $T_\alpha$ . The only non-zero boundary condition for the sensitivities are those at the inlet. Implicit differentiation of  $U_f$  yields the following expressions:

$$S_u^{U_0}(t) = \frac{\partial U_f}{\partial U_0} = 1 + \alpha \sin \frac{2\pi t}{T_\alpha} \quad (24)$$

$$S_u^\alpha(t) = \frac{\partial U_f}{\partial \alpha} = U_0 \sin \frac{2\pi t}{T_\alpha} \quad (25)$$

$$S_u^{T_\alpha}(t) = \frac{\partial U_f}{\partial T_\alpha} = U_0 \alpha \left( -\frac{2\pi t}{T_\alpha^2} \right) \cos \frac{2\pi t}{T_\alpha} \quad (26)$$

$$S_u^{U_0 U_0}(t) = \frac{\partial^2 U_f}{\partial U_0^2} = 0 \quad (27)$$

$$S_u^{\alpha\alpha}(t) = \frac{\partial^2 U_f}{\partial \alpha^2} = 0 \quad (28)$$

$$S_u^{T_\alpha T_\alpha}(t) = \frac{\partial^2 U_f}{\partial T_\alpha^2} = U_0 \alpha \left[ \frac{4\pi t}{T_\alpha^3} \cos \frac{2\pi t}{T_\alpha} - \left( \frac{2\pi t}{T_\alpha^2} \right)^2 \sin \frac{2\pi t}{T_\alpha} \right]. \quad (29)$$

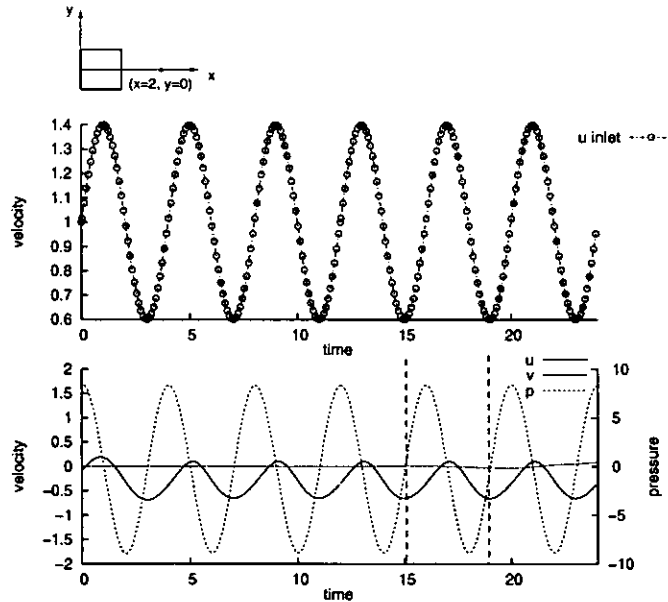


Figure 5. Pulsed flow around a square cylinder: Flow response at  $(x = 2, y = 0)$ .

## 2. Flow response

The harmonic variation of the inflow boundary condition should induce symmetrical vortex shedding. This is exactly what is observed in the flow simulation (see Figures 6). Figure 5 shows the time variation of the inflow velocity and that of the flow (velocity and pressure) at a point located on the symmetry axis one diameter downstream of the cylinder. The signal is shown from time  $t = 0$  for six periods of the inflow variation. Notice that the transverse velocity  $v$  is zero, confirming that the flow and vortex shedding are symmetric with respect to the  $x$ -axis. The axial velocity  $u$  and the pressure  $p$  vary with the period of the inflow boundary condition. The streamwise velocity  $u$  is in phase with the inflow and corresponds to the variations induced by the shed vortices. Notice that the pressure is out of phase by  $\pi/2$  with respect to the inflow.<sup>26</sup>

Vorticity contours are shown on Figure 6 over one period  $T_\alpha$  corresponding to the shaded area on Figure 5. The points on the left-hand curves show the phase in the inflow boundary condition. Two vortices form at the rear corners of the square cylinder during the ascending phases of the pulsation; shedding occurs at the peak of the pulsation. Vortices are transported downstream in the wake during the descending phase while two new vortices start building up. The flow remains symmetric throughout the flow period as can be seen from the straight contours near the symmetry axis. Thus, the dominant phenomena is symmetric vortex shedding induced by the flow pulsation.

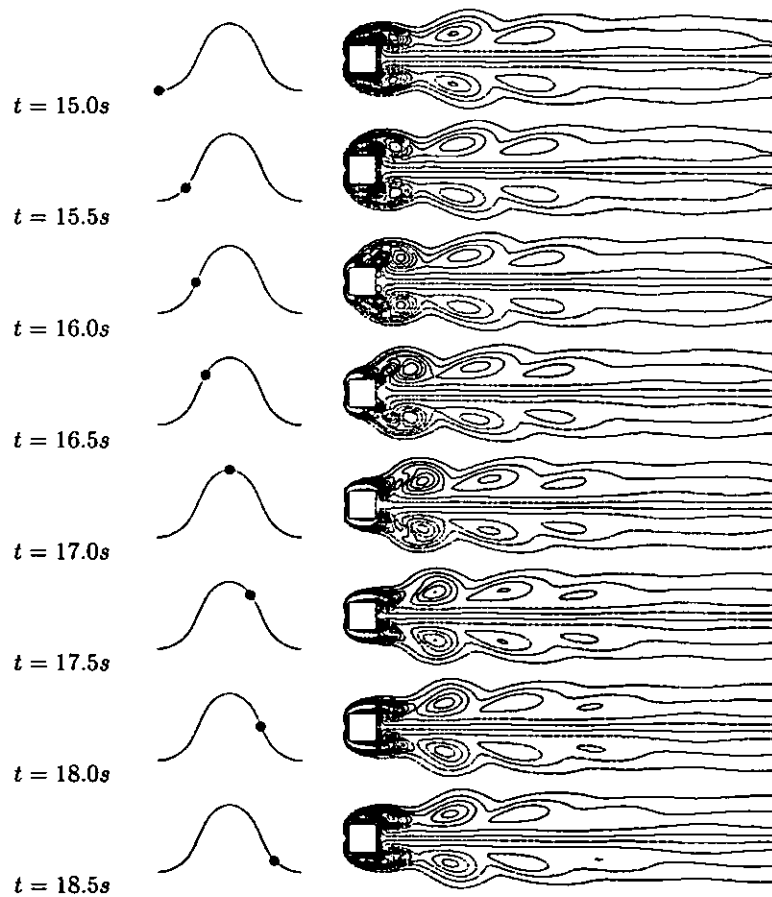


Figure 6. Pulsed flow around a square cylinder: Symmetrical vortex shedding.

By looking carefully at Figure 5 one notices that  $v$  becomes non-zero near the end of the simulation. A trend towards oscillation seems to be developing. The flow is no longer symmetric at time  $t = 24$  and a transition of flow regime is occurring. The simulation was continued for six additional periods  $T_\alpha$ . Vorticity

contours are shown in Figure 7 at times  $t = 32$ ,  $t = 36$ ,  $t = 40$ , and  $t = 44$ . The flow becomes strongly non-symmetric and a Karman vortex street is developing. This is to be expected as the wake of a square cylinder at  $Re = 100$  is an unstable flow. Because the critical Reynolds number for this flow is  $Re_{cr} = 51$ ,<sup>27</sup> a vortex street would develop for constant inflow boundary conditions. Here, the pulsation at the inflow acts as a trigger for vortex shedding. Obviously, the final periodic flow will depend on  $T_\alpha$ , the imposed pulsation period, and the obstacle natural shedding frequency.

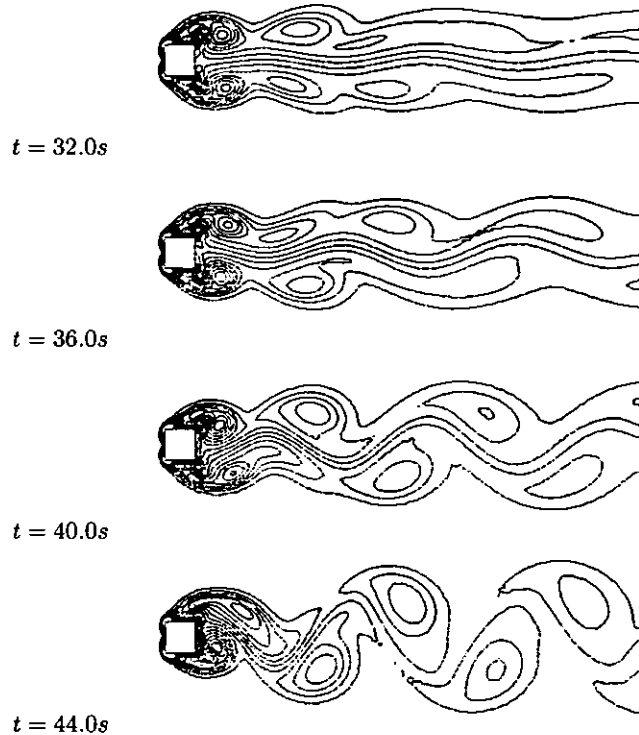


Figure 7. Pulsed flow around a square cylinder: Karman vortex street at later times.

### 3. Flow sensitivity responses

The time signal at  $(x = 2, y = 0)$  of the first and second order flow sensitivities with respect to  $\alpha$ ,  $T_\alpha$  and  $U_0$  are shown in Figures 8, 9 and 10. The solution of the sensitivity equations is compared with the derivative computed by central finite differences with  $\delta a = 0.01a$ . The accuracy of the the finite differences derivatives is of the order of  $O(\delta a^2)$  for both the first and second order derivatives. The following observations can be made:

- The period of the sensitivity signals is  $T_\alpha$ , the period of the inflow pulsation;
- Velocity and pressure sensitivities with respect to  $T_\alpha$  exhibit linearly increasing amplitudes. This is to be expected since the inflow boundary condition for  $S_u^{T_\alpha} = (-2\pi t U_0 \alpha / T_\alpha^2) \cos \frac{2\pi t}{T_\alpha}$  is a linearly increasing function of time;
- The  $v$ -sensitivities are initially small, but they become sizable by the end of the simulation. This is especially visible for  $S_v^{U_0}$  which becomes of the same size as  $S_u^{U_0}$  by the end of the simulation. A similar behavior was observed in the time-signal of  $v$ , the transverse velocity component;
- In all cases the computed sensitivities agree very well with the finite difference derivatives.

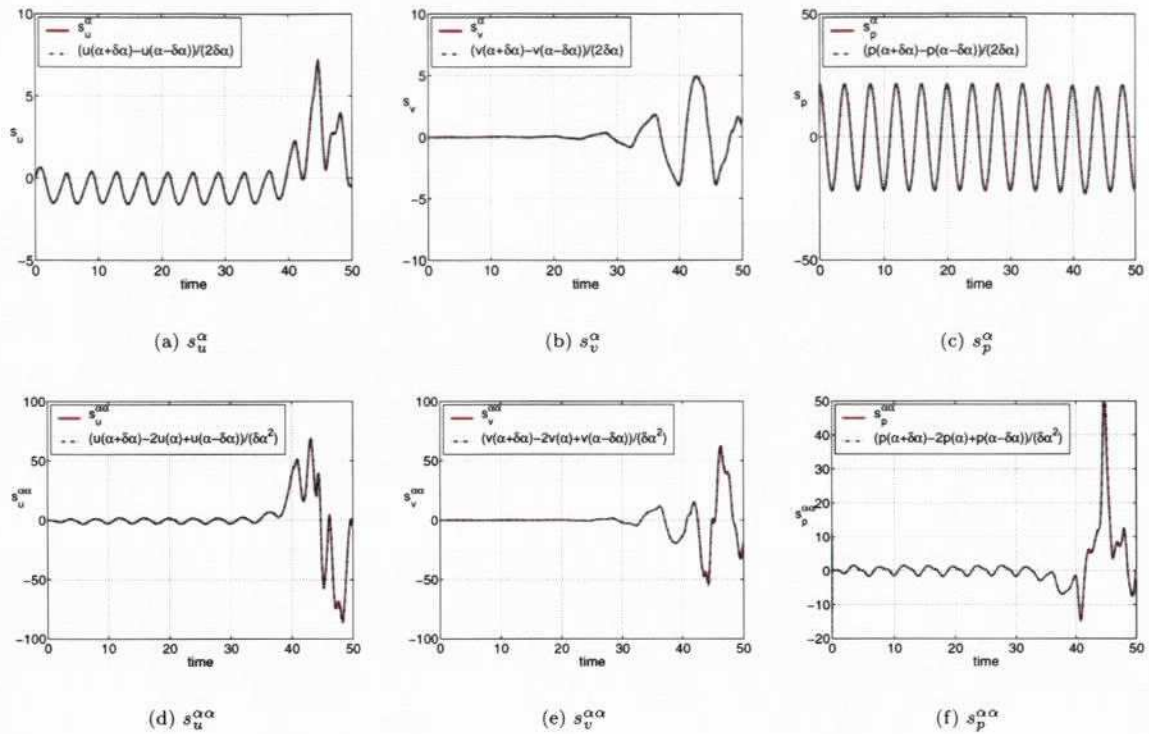


Figure 8. Pulsed flow around a square cylinder: Sensitivities with respect to  $\alpha$  at  $(x = 2.0, y = 0.0)$ .

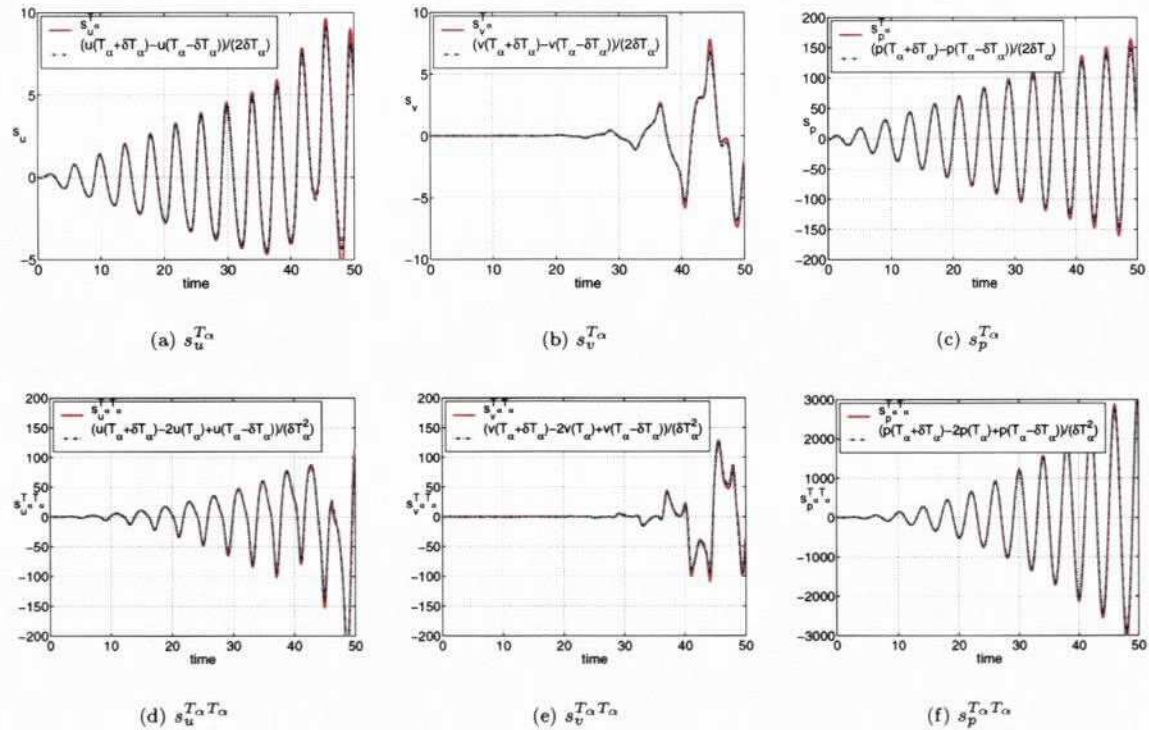


Figure 9. Pulsed flow around a square cylinder: Sensitivities with respect to  $T_\alpha$  at  $(x = 2.0, y = 0.0)$ .

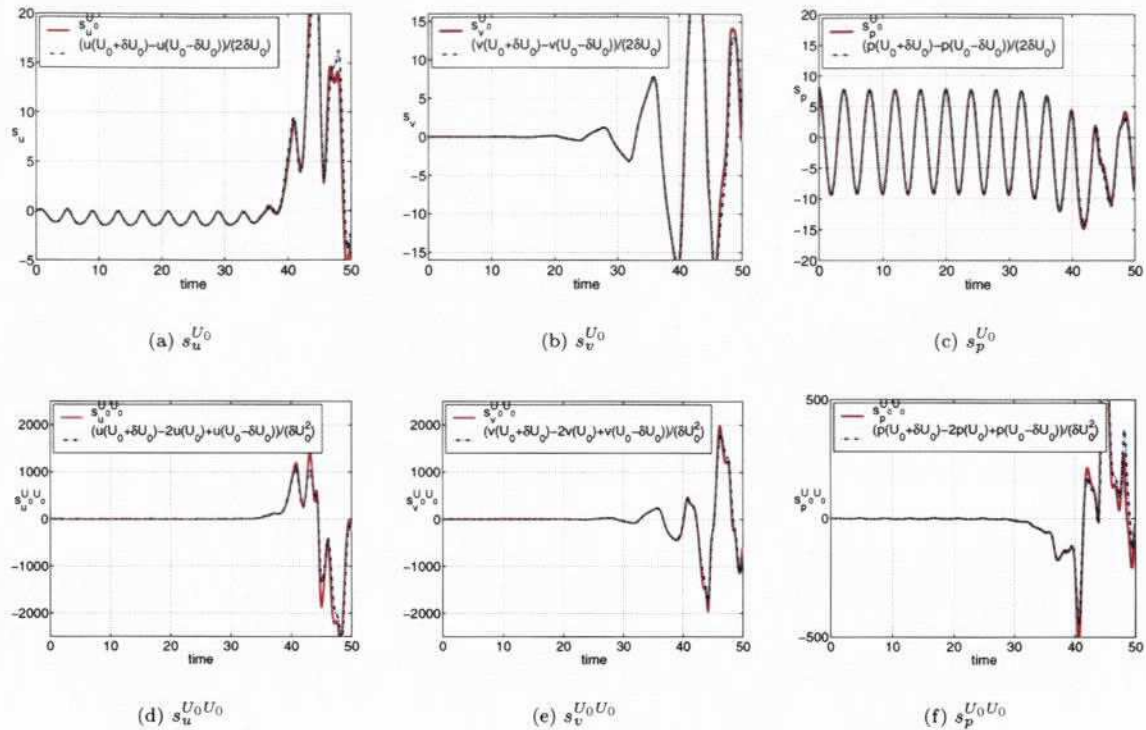


Figure 10. Pulsed flow around a square cylinder: Sensitivities with respect to  $U_0$  at  $(x = 2.0, y = 0.0)$ .

#### 4. Fast evaluation of nearby flows

Sensitivities can be used for fast evaluation of nearby flows. Consider for example what happens to the  $u$ -velocity, when a generic parameter  $a$  is subject to a variation  $\delta a$  from the reference value  $a_0$ . The Taylor series expansion give:

$$u(x, y; a_0 + \delta a) = u(x, y; a_0) + \frac{\partial u}{\partial a} \delta a + \frac{\partial^2 u}{\partial a^2} \frac{\delta a^2}{2} + O(\delta a^3). \quad (30)$$

We use the above parameter perturbations in linear Taylor series and compare estimates of  $u$ ,  $v$  and  $p$  to a full flow analysis at the perturbed values of the parameters. Results obtained using first and second order Taylor series are shown. The reconstructed solutions are very close to those recomputed at the perturbed value of the parameter. Hence, only the errors of the Taylor series with respect to the recomputed solution are shown in Figure 11. The Taylor series approximations of the flow response are in good agreement with the CFD analysis at the perturbed values of the parameters at early times,  $t < 35$ . Agreement deteriorates slightly at later times. In all cases agreement improves when both first and second order sensitivities are used. Agreement is better for perturbations in  $\alpha$  than for perturbations in  $T_\alpha$  and  $U_0$ . In the latter case, the Taylor series still yields good results at early times. The Taylor series estimates are less accurate for  $t > 35$ .

#### C. Pulsed flow around a circular cylinder

The flow problem together with the first and second order sensitivities was also solved for the pulsed flow around a circular cylinder. Figure 12 shows first and second order sensitivities with respect to  $U_0$  and the comparison with central finite difference approximation. As can be seen both first and second order derivatives are accurately computed and the agreement with the finite differences is excellent. This is an improvement over the case of the square cylinder which can be explained by the absence of singularities associated with the corners of the square cylinder geometry.

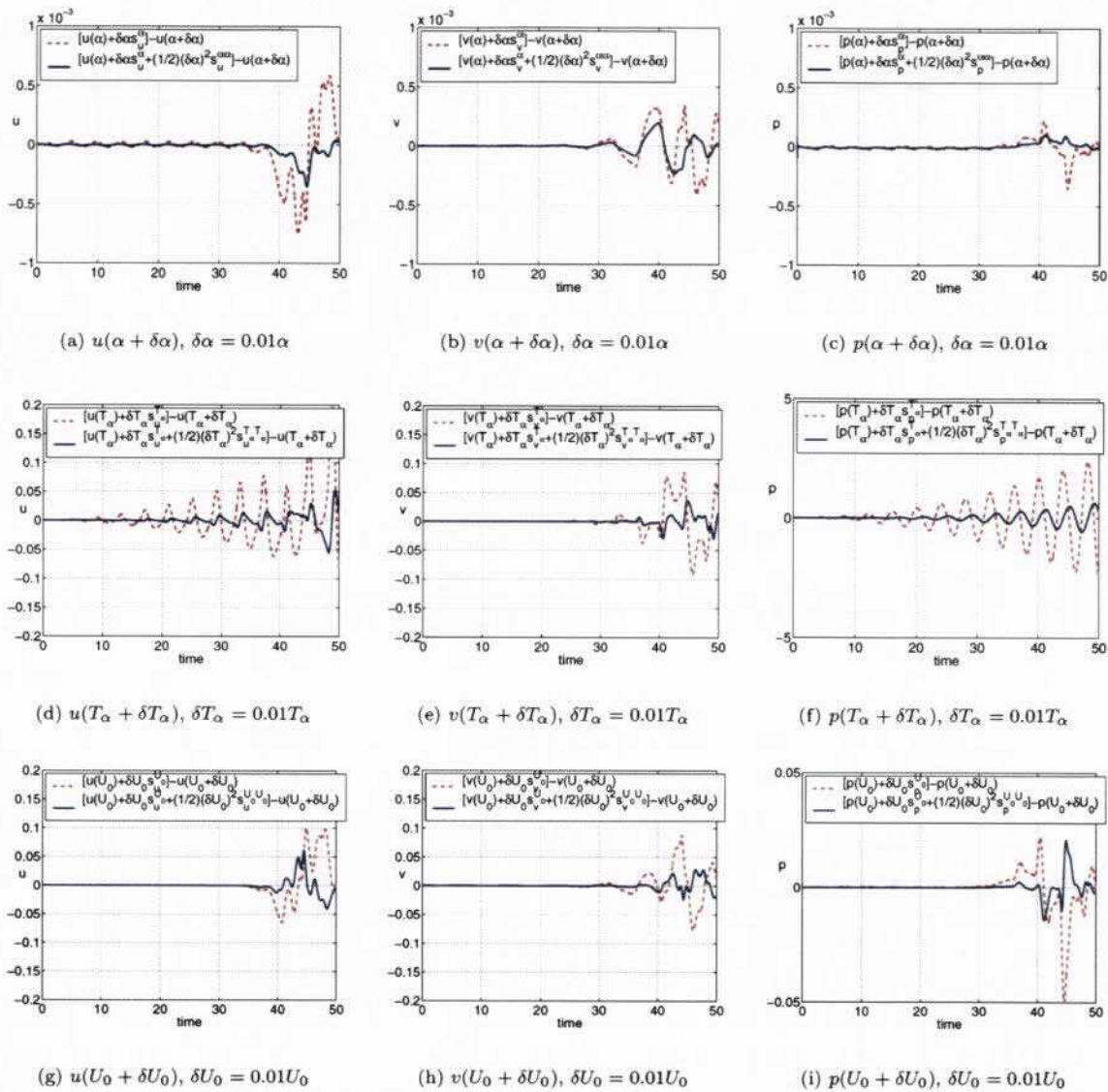


Figure 11. Pulsed flow around a square cylinder: Errors of fast nearby solutions for  $\delta a$  equal to 1% of  $a$  at  $(x = 2.0, y = 0.0)$ .

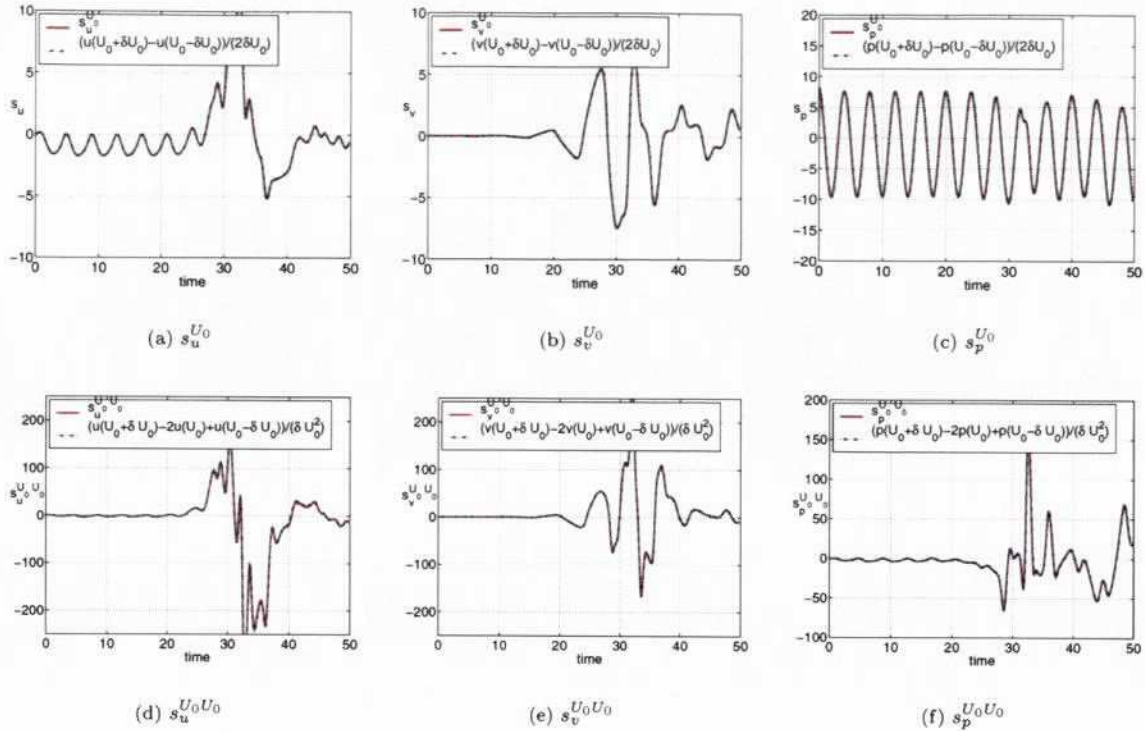


Figure 12. Circular cylinder in pulsed flow at  $(x = 2.0, y = 0.0)$ : Sensitivities with respect to  $U_0$ .

The errors of the fast nearby solutions obtained from Taylor series expansions are shown in Figure 13. Here again, the accuracy of the reconstructed solution improves greatly when both first and second order sensitivities are used in the Taylor expansion. Errors of the reconstructed solution are smaller in the case of the circular cylinder than in the case of the square cylinder.

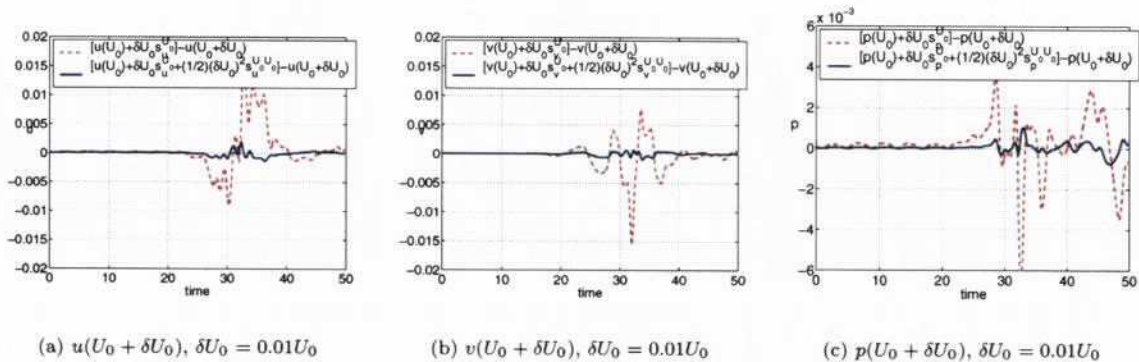


Figure 13. Circular cylinder in pulsed flow at  $(x = 2.0, y = 0.0)$ : Errors of fast nearby solutions.

#### D. Uniform flow around a circular cylinder

For this problem a steady velocity profile was imposed at the inflow. Because the computational domain and mesh are symmetrical with respect to the horizontal axis passing through the center of the cylinder, the vortex street behind the cylinder is difficult to generate. In such circumstances the vortex formation depends on truncation errors and tolerances for the non-linear iterative convergence. In this work we investigate the

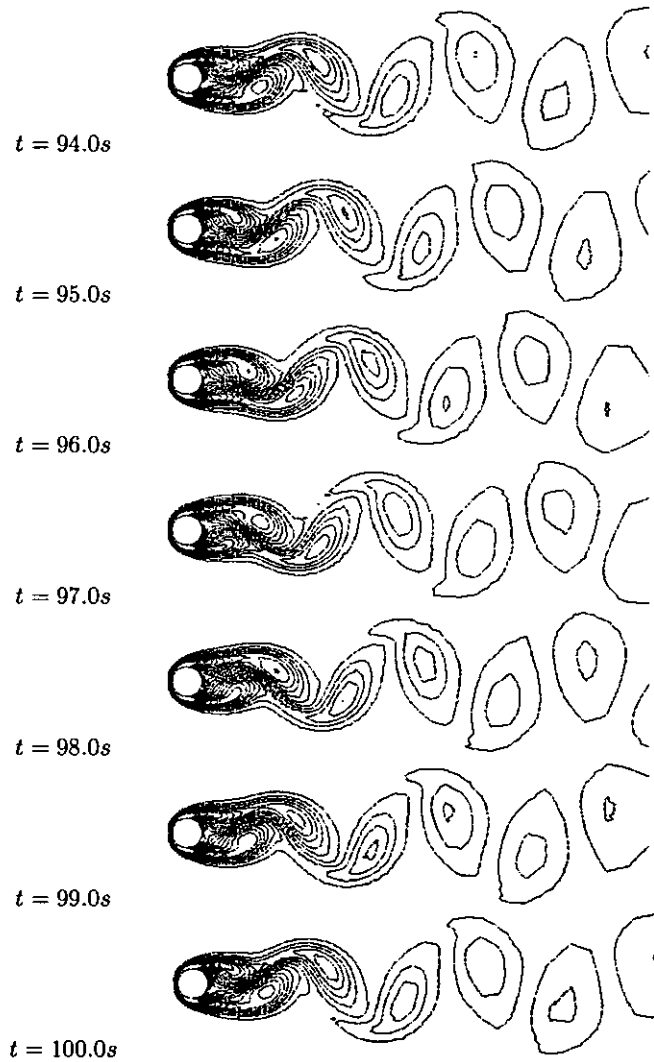


Figure 14. Uniform flow around a circular cylinder: Karman vortex street.

sensitivity of the flow solution and therefore the repeatability of the solution is of paramount importance. The controlled and repeatable vortex street formation is achieved by imposing a slightly non-uniform velocity profile as given by:

$$U_f = U_0 (1 + U_p g(y)) \quad (31)$$

where  $U_0 = 1$  is the value of the free-stream velocity,  $U_p$  is a small perturbation velocity set at  $10^{-3}$  and  $g(y)$  is an anti-symmetric function taking values between -1 and 1. Here we have used the form:

$$g(y) = \tanh(\beta y) \quad (32)$$

with  $\beta = 10$ . This approach ensures that small changes in parameter values will induce small changes in the behavior of the flow.

An initial solution was obtained at  $Re = 100$  using the computational domain with dimensions as shown in Figure 4(a). Vorticity contours are shown in Figure 14 at times  $t = 94$  through  $t = 100$ . The flow is strongly non-symmetric and a Karman vortex street is present in the wake behind the cylinder.

The frequency of the vortex street was analyzed by computing the Strouhal number:

$$St = \frac{fD}{U_0} \quad (33)$$

where  $f$  is the frequency of the vortex shedding and  $D$  is the diameter of the cylinder. The Strouhal number is known to depend upon the Reynolds number of the flow and a correlation of experimental data for the Strouhal-Reynolds relationship was proposed by Williamson.<sup>28</sup> Here, the solution given by the present numerical approach is compared with the correlation of Williamson. The sensitivity of the Strouhal number with respect to the Reynolds number was also obtained from the sensitivity of the flow with respect to the free-stream velocity. Results are shown in Figure 15. Two sets of numerical solutions are plotted. The first

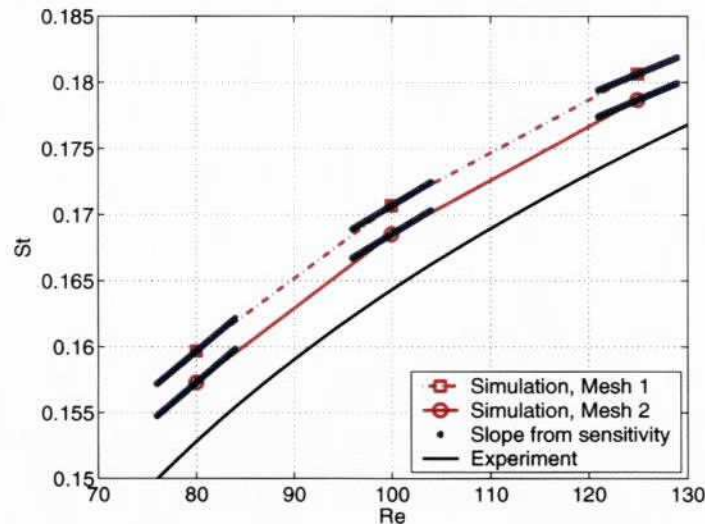


Figure 15. Uniform flow around a circular cylinder: Strouhal dependence upon Reynolds.

one, identified as Mesh 1, corresponds to the solution obtained on a domain of the size shown in Figure 4(a). Behr et al.<sup>29</sup> reported that  $St$  depends on the position of the upper and lower boundaries. Therefore, a second series of computations was carried out on a domain twice as height as that of the Figure 4(a) (Mesh 2). For this configuration of the horizontal boundaries, the solution exhibits little dependence to further changes of the boundary position.<sup>29</sup> As can be seen, the numerical solution overestimates the experimental correlation, but the difference decreases when increasing the size of the computational domain. Note also that the gap between the simulated  $St$  and the experimental values remains the same when varying the Reynolds number, thus indicating that the simulation recovers well the change in  $St$  when  $Re$  changes. The sensitivity of the Strouhal number with respect to  $Re$  was also computed by using the first and second order

sensitivities of the solution with respect to the free-stream velocity (see the blue symbols in Figure 15). As can be seen, the SEM produces results that correctly describe the trend in the  $St - Re$  relationship. The slope of  $St$  computed from the sensitivities agrees very well with the computed and experimental  $St - Re$  relationships. Comparison between the values of  $\partial St / \partial Re$  given by the experimental correlation and the sensitivity analysis are shown in Figure 16. Here again we see that the agreement is good with the experimental observation.

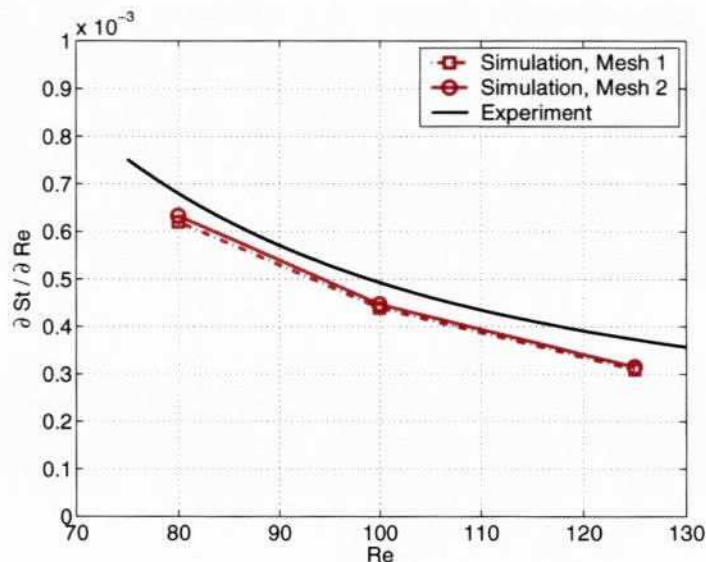


Figure 16. Uniform flow around a circular cylinder: Variation of the slope  $\frac{\partial St}{\partial Re}$  with  $Re$ .

## VI. Conclusion

A general sensitivity equation formulation was developed for the solution of first and second order sensitivities for time-dependent incompressible laminar flows. The method was verified on a problem with a closed form solution to confirm the rate of convergence of the solver for the flow and the first and second order sensitivities.

The method was then applied to pulsed flow around square and circular cylinders. The flow starts with symmetrical vortex shedding due to the harmonic variation of the inflow boundary condition. The flow then goes through a transition phase leading to the usual Karman vortex street characterized by alternate vortex shedding. First and second order sensitivities compare very well with those obtained by finite differences indicating that sensitivity computations are accurate. Sensitivities were also demonstrated as a powerful tool for fast evaluation of nearby flows. Results indicate that accuracy improves when second order sensitivities are included in the Taylor expansion.

The sensitivity analysis was also carried out for the classical uniform flow past a circular cylinder and special emphasis was placed on the sensitivity of the Strouhal number. The slope of the  $St - Re$  relationship computed using sensitivity information agrees well with both the computed and experimental changes of  $St$  with  $Re$  number.

## VII. Acknowledgments

This work was sponsored in part by NSERC (Government of Canada), FQRNT (Government of Québec), the Canada Research Chair Program (Government of Canada), and by the Air Force Office of Scientific Research under grant AFOSR F49620-00-1-0299.

## References

- <sup>1</sup>Martins, J. R. R. A., Stradza, P., and Alonso, J. J., "The complex-step derivative approximation," *ACM transactions on mathematical software - TOMS*, Vol. 29, No. 3, 2003, pp. 245–262.
- <sup>2</sup>Putko, M., Newman, P., Taylor, A., and Green, L., "Approach for uncertainty propagation and robust design in CFD using sensitivity derivatives," *15th AIAA Computational Fluid Dynamics Conference*, Anaheim, CA, June 2001, AIAA Paper 2001-2528.
- <sup>3</sup>Borggaard, J. and Burns, J., "A PDE Sensitivity Equation Method for Optimal Aerodynamic Design," *Journal of Computational Physics*, Vol. 136, No. 2, 1997, pp. 366–384.
- <sup>4</sup>Stanley, L. G. and Stewart, D. L., *Design Sensitivity Analysis: Computational Issues of Sensitivity Equation Methods*, Vol. 25 of *Frontiers in Applied Mathematics*, SIAM, Philadelphia, 2001.
- <sup>5</sup>Turgeon, É., Pelletier, D., and Borggaard, J., "A General Continuous Sensitivity Equation Formulation for Complex Flows," *8th AIAA/NASA/USAF/ISSMO Symposium on Multidisciplinary Analysis and Optimization*, Long Beach, CA, Sep. 2000, AIAA Paper 2000-4732.
- <sup>6</sup>Haug, E. J., Choi, K., and Komkov, V., *Design sensitivity analysis of structural systems*, Vol. 177 of *Mathematics in science and engineering*, Academic Press, Orlando, 1986.
- <sup>7</sup>Hien, T. D. and Kleiber, M., "Stochastic finite element modeling in linear head transfer," *Computer methods in Applied Mechanics and Engineering*, Vol. 144, 1997, pp. 111–124.
- <sup>8</sup>Gunzburger, M. D., *Perspectives in Flow Control and Optimization*, SIAM, 2002.
- <sup>9</sup>Sherman, L. L., Taylor III, A. C., Green, L., Newman, P. A., Hou, G. W., and Korivi, V. M., "First- and second-order aerodynamic sensitivity derivatives via automatic differentiation," *Journal of Computational Physics*, Vol. 129, No. 2, 1996, pp. 307–331.
- <sup>10</sup>Godfrey, A. G. and Cliff, E. M., "Direct Calculation of Aerodynamic Force Derivatives: A Sensitivity-Equation Approach," *36th AIAA Aerospace Sciences Meeting and Exhibit*, Reno, NV, January 1998, AIAA Paper 98-0393.
- <sup>11</sup>Godfrey, A. G. and Cliff, E. M., "Sensitivity Equations for Turbulent Flows," *39th AIAA Aerospace Sciences Meeting and Exhibit*, Reno, NV, Jan. 2001, AIAA Paper 2001-1060.
- <sup>12</sup>Limache, A., *Aerodynamic Modeling Using Computational Fluid Dynamics and Sensitivity Equations*, Ph.D. thesis, Virginia Polytechnic Institute and State University, Blacksburg, VA, 2000.
- <sup>13</sup>Turgeon, É., Pelletier, D., and Borggaard, J., "Computation of Airfoil Flow Derivatives Using a Continuous Sensitivity Equation Method," *8th CASI Aerodynamics Symposium*, Toronto, Canada, April 2001.
- <sup>14</sup>Blackwell, B. F., Dowding, K. J., Cochran, R. J., and Dobranich, D., "Utilization of sensitivity coefficients to guide the design of a Thermal battery," *Proceedings of the 1998 ASME/IMECE*, ASME, Anaheim, CA, 1998, pp. 73–82, HTD-Vol. 561-5.
- <sup>15</sup>Borggaard, J. and Pelletier, D., "Optimal Shape Design in Forced Convection Using Adaptive Finite Elements," *36th AIAA Aerospace Sciences Meeting and Exhibit*, Reno, NV, January 1998, AIAA Paper 98-0908.
- <sup>16</sup>Turgeon, É., Pelletier, D., and Borggaard, J., "A General Purpose Sensitivity Equation Formulation for Complex Flows," *Proceedings of the 8th Annual Conference of the Computational Fluid Dynamics Society of Canada*, Vol. 2, June 11-13, 2000 / Montréal, Canada, pp. 697–704.
- <sup>17</sup>Turgeon, É., Pelletier, D., and Borggaard, J., "A Continuous Sensitivity Equation Method for Flows with Temperature Dependent Properties," *8th AIAA/NASA/USAF/ISSMO Symposium on Multidisciplinary Analysis and Optimization*, Long Beach, CA, Sep. 2000, AIAA Paper 2000-4821.
- <sup>18</sup>Turgeon, É., Pelletier, D., and Borggaard, J., "Application of a Sensitivity Equation Method to the  $k - \epsilon$  Model of Turbulence," *15th AIAA Computational Fluid Dynamics Conference*, Anaheim, CA, Jun. 2001, AIAA Paper 2001-2534.
- <sup>19</sup>Turgeon, É., Pelletier, D., and Borggaard, J., "A General Continuous Sensitivity Equation Formulation for the  $k - \epsilon$  Model of Turbulence," *31st AIAA Fluid Dynamics Conference and Exhibit*, Anaheim, CA, Jun. 2001, AIAA Paper 2001-3000.
- <sup>20</sup>Ilinca, F., Hétu, J.-F., "Three-dimensional Simulation and Design Sensitivity Analysis of the Injection Molding Process," *NUMIFORM 2004*, Columbus, OH, Jun. 2004.
- <sup>21</sup>Turgeon, É., Pelletier, D., and Borggaard, J., "A Continuous Sensitivity Equation Approach to Optimal Design in Mixed Convection," *33rd AIAA Thermophysics Conference*, Norfolk, VA, Jun.-Jul. 1999, AIAA Paper 99-3625.
- <sup>22</sup>Turgeon, É., Pelletier, D., and Borggaard, J., "Sensitivity and Uncertainty Analysis for Variable Property Flows," *39th AIAA Aerospace Sciences Meeting and Exhibit*, Reno, NV, Jan. 2001, AIAA Paper 2001-0139.
- <sup>23</sup>Ilinca, F., Hétu, J.-F., and Pelletier, D., "On stabilized finite element formulations for incompressible flows," *13th AIAA Computational Fluid Dynamics Conference*, Snowmass, Colorado, 1997, AIAA Paper 97-1863.
- <sup>24</sup>Roache, P. J., *Verification and Validation in Computational Science and Engineering*, Hermosa publishers, Albuquerque, NM, 1998.
- <sup>25</sup>Von Schwind, J. J., *Geophysical Fluid Dynamics for Oceanographers*, Prentice-Hall, 1980.
- <sup>26</sup>Hristova, H., Étienne, S., Pelletier, D., and Borggaard, J., "A Continuous Sensitivity Equation Method for Time-Dependent Incompressible Laminar Flows," *34th AIAA Fluid Dynamics Conference and Exhibit*, Portland, OR, Jun. 2004, AIAA Paper 2004-2630.
- <sup>27</sup>Sohankar, A., Norberg, C., and Davidson, L., "Low-Reynolds-Number Flow Around a Square Cylinder at Incidence: Study of Blockage, Onset of Vortex Shedding and Outlet Boundary Condition," *Int. Journal for Numerical Methods in Fluids*, Vol. 26, 1998, pp. 39–56.
- <sup>28</sup>Williamson, C. H. K., "Defining a universal and continuous Strouhal-Reynolds number relationship for the laminar vortex shedding of a circular cylinder" *Phys. Fluids*, Vol. 31, 1988, pp. 2742–2744.
- <sup>29</sup>Behr, M., Hastreiter, S., Mittal, S., and Tezduyar, T. E., "Incompressible flow past a circular cylinder: Dependence of the computed field on the location of the lateral boundaries", Vol. 123, 1995, pp. 309–316.